JACS
JOURNAL OF THE AMERICAN CHEMICAL SOCIETY

Article

pubs.acs.org/JACS

A New Class of Electrocatalysts for Hydrogen Production from Water Electrolysis: Metal Monolayers Supported on Low-Cost Transition Metal Carbides

Daniel V. Esposito, Sean T. Hunt, Yannick C. Kimmel, and Jingguang G. Chen*

Department of Chemical Engineering, University of Delaware, Newark, Delaware 19716, United States

Supporting Information

ABSTRACT: This work explores the opportunity to substantially reduce the cost of hydrogen evolution reaction (HER) catalysts by supporting monolayer (ML) amounts of precious metals on transition metal carbide substrates. The metal component includes platinum (Pt), palladium (Pd), and gold (Au); the low-cost carbide substrate includes tungsten carbides (WC and W_2C) and molybdenum carbide (Mo_2C). As a platform for these studies, single-phase carbide thin films with well-characterized surfaces have been synthesized, allowing for a direct comparison of the intrinsic HER activity of bare and Pt-modified carbide surfaces. It is found that WC and W_2C are both excellent cathode support materials for ML Pt, exhibiting HER activities that are comparable to bulk Pt while displaying stable HER activity during chronopotentiometric HER measurements. The findings of excellent stability and HER activity of the ML Pt−WC and Pt−W_2C surfaces may be explained by the similar bulk electronic properties of tungsten carbides to Pt, as is supported by density functional theory calculations. These results are further extended to other metal overlayers (Pd and Au) and supports (Mo_2C), which demonstrate that the metal ML-supported transition metal carbide surfaces exhibit HER activity that is consistent with the well-known volcano relationship between activity and hydrogen binding energy. This work highlights the potential of using carbide materials to reduce the costs of hydrogen production from water electrolysis by serving as stable, low-cost supports for ML amounts of precious metals.

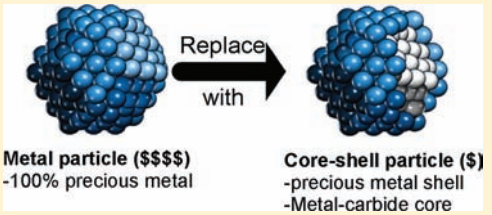

1. INTRODUCTION

Using electrons generated from renewable energy sources, the production of hydrogen from the electrolysis of water is a promising alternative to the current CO_2-emitting fossil fuel based energy system.[1] At low temperatures, the electrolysis can take place in an electrolyzer or photoelectrochemical cell, in which the oxygen evolution (OER) and hydrogen evolution (HER) reactions occur at the anode and cathode of the device, respectively. Currently, the low-temperature electrolyzer market is dominated by alkaline and proton exchange membrane (PEM) electrolyzers.[2] Alkaline electrolysis is the more established technology and benefits from the ability to use nonprecious metal catalysts at high pH values, but produces H_2 at lower pressures and necessitates the use of hazardous potassium hydroxide (KOH) as an electrolyte. In PEM electrolyzers, the caustic KOH electrolyte is replaced with an acidic, proton-conducting solid electrolyte membrane, such as Nafion. Compared to alkaline electrolysis, PEM electrolyzers can produce hydrogen at higher outlet pressures, higher purity levels, and with lower maintenance requirements.[3] However, the electrolysis efficiency in acidic conditions suffers unless costly precious metals are used, such as Pt.[3] In addition to being expensive, estimated global Pt reserves are extremely low, making it improbable that a worldwide fleet of fuel cell vehicles and PEM electrolyzers can be produced using present Pt loadings.[4] To overcome this challenge and drive down the cost of H_2 production from water electrolysis, it is necessary to dramatically decrease or eliminate the loading of Pt in these devices.

One class of low-cost catalytic materials with great potential for replacing or reducing Pt in HER applications is transition metal carbides (TMC), which are known to display similar electronic and catalytic properties to Pt-group metals.[5] Equally important, the transition metals used in commonly explored TMC catalysts (Ti, V, Mo, Ta, W) are orders of magnitude more abundant[6] and less expensive[7,8] than Pt-group metals (Ru, Rh, Pd, Ir, Pt). On the basis of cost comparisons, it is evident that the replacement or reduction of precious metal loading with TMCs offers great opportunity for cost reduction in electrocatalytic applications such as water electrolysis.

Among TMC materials, WC and W_2C electrodes are especially promising candidates to be used in HER applications because they are known to exhibit good stability in acidic environments[9−11] and have shown sufficient HER activity to be considered as stand-alone HER electrocatalysts.[12−15] However, the reported HER catalytic activities of WC and W_2C, expressed in terms of exchange current density (i_o), are still 2−3 orders of magnitude below many Pt-group metals. For this reason, there has been interest in combining WC and W_2C with Pt-group metals as co-catalysts,[16−18] with several studies reporting that WC/W_2C powder-supported Pt particles show significantly higher HER activity than conventional carbon-

Received: September 14, 2011
Published: January 12, 2012

   dx.doi.org/10.1021/ja208656v | J. Am. Chem.Soc. 2012, 134, 3025−3033

supported Pt particles. The primary motivation for combining Pt with WC/W_2C is that the similarities in the electronic structures result in good adhesion and synergistic chemistry. However, many conclusions of the aforementioned HER studies on supported Pt and WC/W_2C particles are hindered by questions regarding the phase purity, powder surface area, differences in Pt particle dispersion, and the relative location of Pt and WC/W_2C particles on the catalyst support. Because of variation in so many parameters, it has been difficult to conclusively determine (i) why Pt−WC/W_2C catalysts show higher activity than comparable Pt−C catalysts, (ii) which carbide phase (or combination of phases) is optimal for supporting Pt for HER applications, and (iii) whether Pt particles are in direct contact with WC/W_2C to achieve the claimed synergistic effect.

There are two primary objectives in the present study. First, we seek to elucidate some of the aforementioned questions regarding the Pt−WC/W_2C HER catalysts by studying precious metal HER electrocatalysts deposited on smooth, single-phase WC/W_2C thin films with well-controlled surface stoichiometry. The use of single-phase TMC thin films having comparable surface areas allows for direct comparisons of the HER activity and stability of these surfaces, and allows for much more meaningful kinetic analysis of TMC and metal-modified TMC catalysts. Thin films also represent a great platform to investigate the catalytic activity of so-called "monolayer bimetallic catalysts", which consist of one atomic layer, or monolayer (ML), of a metal supported on a substrate material. ML-bimetallic catalysts have received much attention in recent years for their potential to improve catalytic activity and stability,[19] and offer the ability to drastically reduce catalyst cost when a low-cost substrate is used. In a recent communication,[20] we demonstrated the usefulness of this approach by exploring the HER activity of sub-ML to ML amounts of Pt deposited on single-phase WC thin films. Although the HER activity of ML Pt−WC was shown to be comparable to bulk Pt, the more critical question of the electrochemical stability of ML Pt−WC was not addressed in detail. In the current study, we have combined DFT predictions and several experimental measurements to evaluate the stability of single-phase WC, W_2C, ML Pt−WC, and ML Pt−W_2C films.

The second objective of this study is to expand the search for low-cost HER catalysts to other TMC-supported ML metals. In addition to WC and W_2C, TMCs such as Mo_2C, TaC, VC, and TiC are also known to display electronic properties similar to Pt-group metals, meaning that other combinations of ML metals and TMCs may also prove to be active, stable electrocatalysts. As a basis for this study, we utilize a DFT-calculated chemical descriptor to predict which combinations of metals and TMCs are active HER catalysts. This approach has proven to be very effective for screening many combinations of bimetallic materials in several electrocatalytic systems.[21−23] We have used a similar theory-guided approach in the current study to investigate the HER activity of a variety of ML-metal TMC surfaces in order to identify trends in HER activity for this class of catalysts. On the basis of these results, opportunities and challenges in the development of low-cost ML metal-TMC HER catalysts are discussed.

The current paper presents several novel concepts that could potentially be of great significance to the production of hydrogen from the electrolysis of water: (1) theoretical prediction and experimental verification of monolayer metal/carbide as low-cost electrocatalysts; (2) proof-of-principle demonstration of enhanced stability between monolayer precious metal with carbide substrates; and (3) confirmation of the validity of using hydrogen binding energy as a descriptor to predict active HER catalysts in the carbide-based electrocatalysts.

2. EXPERIMENTAL AND MODELING METHODS

2.1. Density Functional Theory (DFT) Calculations. Hydrogen and metal−metal (M−M) binding energies were calculated for the close packed crystal structures of all surfaces using the Vienna ab initio Simulation Package (VASP), as described previously.[20] TMC surfaces were composed of three layers of carbides and 12 layers of vacuum, while all other surfaces contained four layers of atoms and 10 layers of vacuum. In all cases, the model surface consisted of a 3×3 surface cell configuration in which the bottom layers were fixed while the top two layers were allowed to relax. A $3 \times 3 \times 1$ Monkhorst-Pack automatic k-point mesh and a plane wave cutoff of 396 eV were used. From DFT results, hydrogen binding energy (HBE) values were calculated as defined by Norskov et al.[24] The M−M binding energies were calculated in the same manner as HBE, but treating the top metal ML as the adsorbate layer. For both HBE and M−M binding energies, the value corresponding to the most stable binding site was used.

2.2. Synthesis of WC, W_2C, and Mo_2C Thin Films. WC and W_2C thin films were deposited on polycrystalline tungsten foil (99.95% pure, Alfa Aesar) by Magnetron sputtering. This procedure involved nonreactive and reactive sputtering using a WC target (99.5% pure) to produce single-phase W_2C and WC thin films, respectively. Single-phase Mo_2C thin films were synthesized by directly carburizing molybdenum foil (99.95% pure, Alfa Aesar) in a quartz tube furnace in the presence of hydrogen and methane. More details on synthesis procedures are provided in Supporting Information.

2.3. Deposition of Pt Overlayers. Pt deposition was carried out using a hot filament Pt source in an XPS chamber with a base pressure of 5×10^{-10} Torr. The Pt source consists of Pt wire (99.99% pure, Alfa Aesar) wrapped tightly around a resistively heated W wire filament, as often used for deposition of metal overlayers with monolayer thickness.[19] For Pt overlayer growth experiments, the substrate was positioned in front of the Pt source for a set amount of time before being transferred to the main chamber where XPS measurements were conducted.

2.4. Characterization Techniques. Scanning Electron Microscopy (SEM) images were taken using a JSM 7400f SEM with an accelerating voltage of 3 KeV and a probe current of 10 μA. Symmetric X-ray diffraction (XRD) was conducted using a Phillips X'Pert PW3040-MPD X-ray diffractometer, operated with a Cu Kα X-ray source at 45 kV and 40 mA. Glancing incidence XRD (GIXRD) was performed using a Rigaku D/Max 2200 diffractometer with a Cu Kα source operated at 40 mA and 40 kV, with the incidence angle set at 1.0, 2.0, or 5.0°.

A Phi 5600 X-ray photoelectron spectroscopy (XPS) system with a multichannel hemispherical analyzer and Al anode X-ray source was used to monitor the growth of Pt overlayers, determine overlayer thickness, and investigate the stability of the substrate and overlayer materials. The XPS was calibrated using the reported binding energies[25] for the strongest photoelectron lines of Au, Ag, and Cu reference foils. Detailed description of the fitting procedure used for determination of XPS peak areas and atomic concentrations of carbide surfaces is provided in the Supporting Information.

2.5. Electrochemical Measurements. The 0.5 M H_2SO_4 (Fisher Scientific, 96.9%) solutions were freshly prepared from deionized water prior to all electrochemical measurements. For quantitative measurement of HER activities in Ar-saturated 0.5 M H_2SO_4, electrodes having areas of 0.75−1.0 cm^2 were assembled with a 1.0 mm thick Teflon sheet epoxied to the backside of the electrodes. Electrochemical measurements were performed in a standard electrochemical cell using a PARSTAT 2273 potentiostat, saturated calomel reference electrode (SCE, −0.241 V vs NHE), and a 10 cm^2 Pt gauze auxiliary electrode. Prior to experiments, H_2SO_4 solutions were purged with high purity Ar for at least 45 min, and a slow flow of Ar was

dx.doi.org/10.1021/ja208656v | J. Am. Chem.Soc. 2012, 134, 3025−3033

maintained above the solution during measurements. Upon submersion in the electrolyte, electrodes were conditioned by conducting 25 cycles of potential cycling between 0.0 and +0.3 V with a scanning rate of 50 mV/s. Linear sweep voltammograms (LSV) were then conducted at a scan rate of 2 mV/s from a starting potential of +0.14 V to a final potential of −0.4 V versus SCE. The stability was evaluated with chronopotentiometric (CP) cycling conducted in H_2-purged 0.5 M H_2SO_4 in a standard two-neck electrochemical cell. A complete description of the setup and procedure used for the two-hour HER stability test is provided in the Supporting Information.

3. RESULTS AND DISCUSSION

3.1. Using DFT To Predict Active and Stable ML TMC HER Catalysts. One of the fundamental concepts of heterogeneous catalysis is Sabatier's principle, whereby those metals that bond reactive intermediates with moderate strength are generally observed to be the most active catalyst toward the reaction.[26] For simple reactions such as the HER that have one key reactive intermediate (adsorbed H), this principle manifests itself in the form of a volcano relationship between HER activity and hydrogen binding energy (HBE).[24,27,28] Based on this correlation, Greeley and co-workers utilized DFT-calculated HBEs to computationally screen over 900 combinations of ML-bimetallic and intermetallic catalysts for the purpose of identifying active HER electrocatalysts.[21] While that study and several others have successfully utilized this computational approach to identify HER catalysts, they have not identified a ML bimetallic surface with nonprecious metal substrate that matches the activity and stability of the standard HER catalyst, Pt. One possible reason for the lack of identifiable nonprecious metal supports for ML Pt-group metals is that the latter generally need to bond to a substrate having similar electronic structure in order to maintain its high catalytic activity and stability. Conversely, it can be expected that a ML of a Pt-group metal bonded to a substrate with substantially different electronic structure would experience a large perturbation in its original electronic structure, leading to large deviation in activity and stability compared to the parent metal. From this reasoning, it follows that the similar electronic properties of many TMCs to Pt-group metals make the former excellent candidates to be low-cost supports for the latter.

In Table 1, DFT-calculated HBE values for several unmodified and ML metal-modified TMC surfaces are shown in comparison to the precious metals Pt and Pd, two of the most active monometallic HER electrocatalysts whose HBEs are located slightly to the left of the center of the HER volcano curve.[24] Although the unmodified TMC surfaces are all predicted to bind hydrogen too strongly compared to Pt and Pd, it is seen that the HBE values of several ML surfaces are located in the optimal HBE range of the volcano curve, approximately −0.1/+0.2 eV less/greater than the HBE of Pt.[24] The finding of similar HBE values, such as between ML Pt−WC and Pt, can be attributed to minimal strain and ligand effects on the Pt ML due to the general similarity between bulk Pt and WC. Also included in Table 1 are the HBE values of several Au surfaces. Although Au is not a prominent HER catalyst, the weak HBE values of the Au surfaces make them useful for analyzing surfaces on both sides of the volcano curve.

Table 1. DFT-Calculated Binding Energies for Hydrogen (HBE) on Various Metal, TMC, and ML M−TMC Surfaces[a]

class	surface	HBE/eV
Carbides	WC(0001)	−0.99
	W_2C(0001)	−0.67
	Mo_2C(0001)	−0.79
Metals	Pt(111)	−0.46
	Au(111)	0.13
	Pd(111)	−0.50
ML M−TMC	ML Pt−WC	−0.43
	ML Pt−W_2C	−0.24
	1 ML Pd−Mo_2C	−0.46
	1 ML Pd−WC	−0.40
	1 ML Au−Mo_2C	0.30
	1 ML Au−WC	−0.06

[a]HBE values were calculated on the close packed surfaces of all surfaces for 1/9 ML H as described in the Experimental and Modeling Methods.

In addition to predicting catalytic activity from the binding energies of reactive intermediates, DFT can also be used to gauge the relative interfacial stability of ML bimetallic catalysts[21,29] and ML core−shell structures.[30] In this work, the relative interfacial stability of various ML M−TMC surfaces is compared by calculating the differences in binding energies of a metal ML with its bulk parent metal (M−M) and with the TMC substrate (M−TMC). In general, ML systems with M−TMC binding energies greater than the M−M binding energy should favor 2-D growth of the metal, producing a ML configuration on the TMC substrates. Conversely, it can be expected that ML systems with M−M binding energies greater than that of the corresponding M−TMC binding energies should experience a driving force toward 3-D agglomeration into bulk-like metal particles.[31,32] In Table 2, DFT-calculated M−M and M−TMC binding energies are listed for Pt, Pd, and Au MLs. Also included are the calculated binding energies for the metal MLs on model graphite C(0001) surfaces (M−C surfaces). Comparison of M−C to M−TMC binding energies are useful since carbon is a commonly used support material in electrocatalytic applications. The absolute and relative magnitudes of the M−M BEs are in good agreement with corresponding bulk metal cohesive energies,[33] while the M−C BEs are consistent with a recent study on ML metal−supported graphene surfaces.[32] Focusing first on the M−TMC binding energies of Table 2, it is seen that these are 15−35% greater

Table 2. DFT-Calculated Binding Energies for 1 ML of Pt, Pd, or Au on Close Packed Surfaces of the Parent Metals (M−M BE), Three Different TMC Surfaces (M−TMC BE), and on Graphite (M−C BE)[a]

ML surface atoms	substrate	binding energy/eV	(M−X*)−(M−M) BE/eV
Pt	Pt(111)	−5.43	0.00
	C(0001)	−4.12	1.31
	WC(0001)	−6.59	−1.16
	W_2C(0001)	−6.51	−1.08
Pd	Pd(111)	−4.68	0.00
	C(0001)	−3.27	1.41
	Mo_2C(0001)	−5.46	−0.78
	WC(0001)	−5.59	−0.91
Au	Au(111)	−2.91	0.00
	C(0001)	−1.60	1.30
	Mo_2C(0001)	−3.90	−1.00
	WC(0001)	−3.69	−0.78

[a]X* refers to the substrate material (TMC or C).

dx.doi.org/10.1021/ja208656v | J. Am. Chem.Soc. 2012, 134, 3025−3033

than the corresponding M−M binding energies, meaning 2-D layer-by-layer growth should be favored on these surfaces. However, the binding energies of ML Pt, Pd, and Au on the graphite C(0001) surface are 24−45% less than M−M binding energies. The disparity in binding energies between the M−C and M−TMC surfaces predicts that the TMC surfaces should serve as more favorable supports for precious metal MLs than conventional carbon. Experimental investigation of the growth and stability of ML Pt on WC and W_2C surfaces is presented and discussed in the following sections.

3.2. Characterization of Pt−WC/W_2C Thin Films. *3.2.1. Thin Film Morphology.* In Figures 1a,b, the

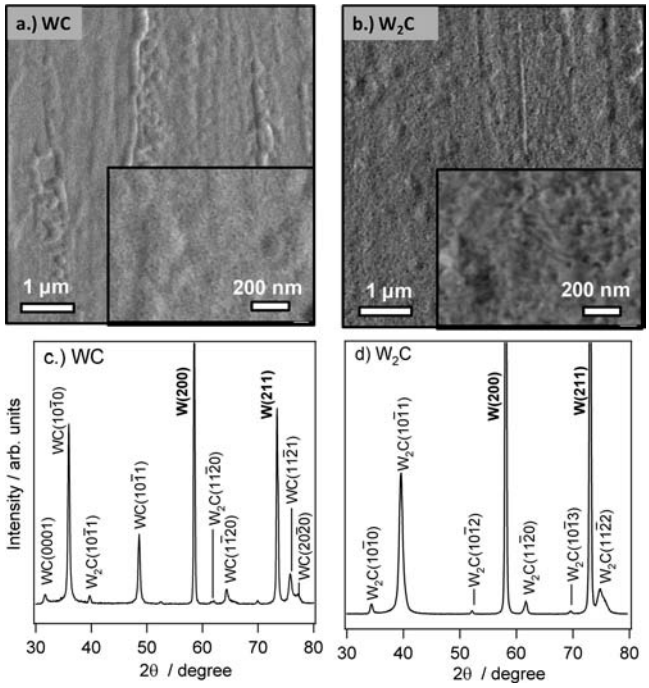

Figure 1. SEM images of as-synthesized PVD thin films of (a) WC and (b) W_2C deposited onto polycrystalline W foil. Symmetric XRD patterns for as-synthesized (c) WC and (d) W_2C thin films.

microscopic surface morphology is shown in SEM images at two different resolutions for each sample. The thin film surfaces are observed to be flat at the micrometer length scale, with the exception of randomly spaced striations directed vertically in Figure 1. These striations are most likely artifacts of milling lines in the W foil substrate, features that are common in the manufacture of metal foils.[34] On the nanoscale, the WC and W_2C thin films appear to have a similar roughness and are characterized by small, barely discernible grains. On the basis of SEM images and electrochemical evidence provided in the Supporting Information, the surface areas of the WC and W_2C thin films are comparable.

3.2.2. Crystal Structure of Carbide Thin Films. XRD and GIXRD were used to verify the bulk crystal structure of as-synthesized thin films, with XRD patterns for the as-synthesized WC and W_2C thin films provided in Figure 1, panels c and d, respectively. For both thin films, the primary diffraction peaks of the W foil substrate are detected at d = 2.238 Å (2θ = 40.3°), d = 1.582 Å (2θ = 58.6°), and d = 1.292 Å (2θ = 72.8°), corresponding to the W (110), W (200), and W (211) crystal planes of unstrained cubic W, respectively [ICDD 04-0806]. In Figure 1c, the XRD pattern of the annealed, reactively sputtered thin film is seen to be consistent with hexagonal WC [ICDD 03-065-4539]. Phase-purity is observed with the exception of very minor $W_2C(10\bar{1}1)$ and $W_2C(10\bar{2}0)$ peaks, which arise from a small amount of W_2C located at the interface between the W foil substrate and WC thin film, as previously shown for carburized WC foils.[35] In Figure 1d, the diffraction pattern for the annealed, nonreactively sputtered thin film is shown, with the peaks corresponding to hexagonal W_2C with space groups $P\bar{3}1m$ [ICDD 01-079-0743] and $P\bar{3}m1$ [ICDD 00-035-0776]. GIXRD patterns for WC and W_2C thin films confirm the single-phase nature near the surface. GIXRD results, along with detailed analysis of the crystal orientation of the thin films, are presented in the Supporting Information.

3.2.3. Characterization of WC/W_2C Surface Stoichiometry. Of great importance to this study is the TMC surface stoichiometry, which is known to have a profound effect on the catalytic behavior of TMC surfaces.[36−38] For example, excess surface carbon has commonly been observed on as-synthesized Pt−WC/W_2C surfaces, and generally has a prohibitive effect on the catalytic properties of a catalyst. In this study, buildup of excess surface carbon was avoided by shutting off the flow of CH_4 during a post deposition annealing step, which has previously been used to eliminate excess surface carbon in the synthesis of WC powder catalysts.[39] Figure 2a

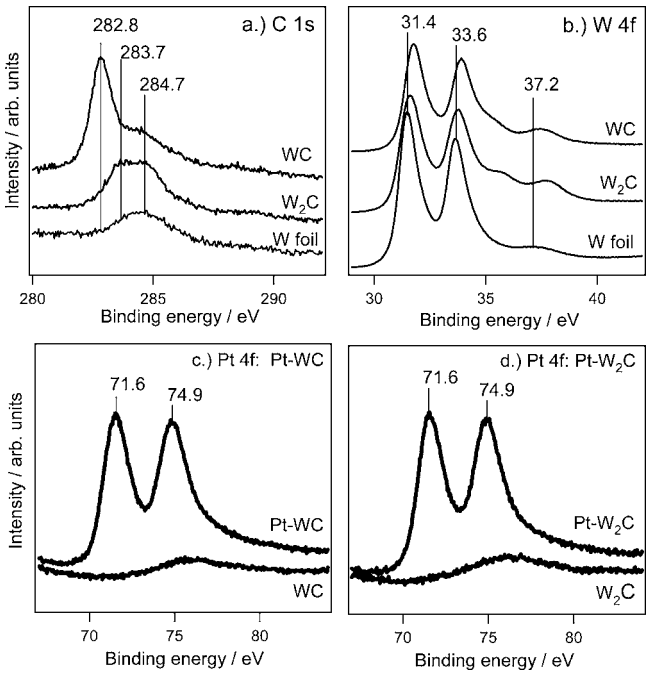

Figure 2. XPS C 1s peaks for as-synthesized (a) PVD WC and (b) PVD W_2C thin films. Spectra for a NaOH-cleaned W foil (bottom spectra) are shown for reference. XPS Pt 4f spectra for 1 ML of Pt deposited on (c) WC and (d) W_2C thin films. Background spectra for unmodified carbide surfaces are also included.

contains XPS C 1s spectra for WC and W_2C thin films for which the CH_4 flow rate was turned off toward the end of the post anneal process. The characteristic carbidic carbon peak for WC is observed at 282.8 eV, while that for W_2C, which is expected to be lower in intensity and higher in binding energy than WC,[38] is located near 283.7 eV. For both WC and W_2C surfaces, small C 1s peaks at 284.7 eV are also observed, which originate from adventitious carbon adsorbates from atmos-

dx.doi.org/10.1021/ja208656v | J. Am. Chem.Soc. 2012, 134, 3025−3033

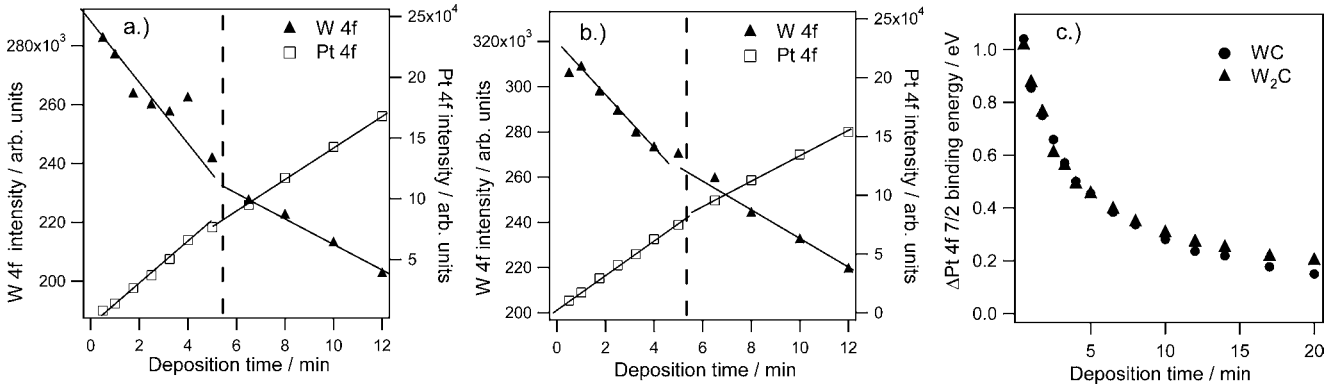

Figure 3. W 4f and Pt 4f intensities versus deposition time for (a) WC and (b) W_2C substrates. (c) XPS Pt $4f_{7/2}$ peak position as a function of time. Peak positions are shown relative to that of a clean Pt foil.

phere. This is confirmed by the similar position and magnitude of the C 1s peak measured on a clean, 99.99% pure W foil.

Figure 2b contains the W 4f spectra of as-synthesized WC and W_2C thin films alongside that of a reference W foil stripped of oxides with aqueous NaOH. The W 4f signals for the W foil sample are located at 31.45 and 33.7 eV, in agreement with literature.[25] The relatively weak and broad peak centered at 37.2 eV is mostly W $5p^3/_2$ signal, not to be confused with W 4f signal originating from W_xO_y species. For all samples, the W 4f peak locations are observed to be shifted +0.2 to 0.4 eV higher in binding energy compared to metallic W. Weak W_xO_y W 4f signals are observed for the carbide samples, likely due to exposure to air during sample transfer from synthesis to XPS measurements. The carbidic W/C atomic ratio of the WC thin film is around 1.0 and that of W_2C around 2.0, as expected for stoichiometric W-carbides.

3.2.4. Quantification of Pt Overlayer Thickness. In Figure 2, panels c and d, XPS of Pt 4f peaks are shown for one ML of Pt deposited on WC and W_2C, respectively. The Pt 4f region for each sample before Pt deposition is also included for comparison, which shows the presence of a broad peak centered at ~75.7 eV that corresponds to signal from a W 4f satellite peak originating from the WC/W_2C substrate. On the basis of the integrated peak areas of the Pt 4f and W 4f features of as-deposited Pt–WC and Pt–W_2C samples, the thickness of the Pt overlayers was estimated using overlayer equations based on the Beer–Lambert law, as described previously.[20] After deposition of 1 ML of Pt on the WC/W_2C thin films, neither the carbidic C 1s spectra nor atomic W/C ratio was observed to change significantly. These results, included in the Supporting Information, suggest that evaporative deposition of Pt used in these studies did not lead to a phase change in the WC/W_2C substrate.

3.2.5. Evidence of ML Pt Formation on Pt–WC/W_2C Surfaces. To investigate the structure of the Pt overlayers deposited on W_xC surfaces, Pt overlayer growth experiments were performed in which the Pt 4f and W 4f spectra were periodically measured during overlayer growth. Figures 3, panels a and b, contain integrated Pt 4f and W 4f peak area intensities as a function of Pt deposition time on WC and W_2C thin films, respectively. For both substrates, changes in the slopes of the Pt 4f and W 4f signals are observed around 5 min of cumulative deposition time. This distinct break in slope is caused by self-screening of successive MLs and is indicative of layer-by-layer overlayer growth.[40] This result is consistent with a similar Pt growth experiment on carburized polycrystalline W surface, in which it was found that layer-by-layer growth persisted for the first two MLs of evaporated Pt.[41]

Further evidence of the ML character of the as-deposited Pt overlayer is the core level shift (CLS) of the Pt 4f $^7/_2$ peak center position relative to that of bulk Pt. CLS values are commonly observed for ultrathin metal overlayers, and are well-known to be dependent on the structure of the metal overlayer.[42] In Figure 3c, the Pt 4f $^7/_2$ peak center position measured throughout the Pt–WC and Pt–W_2C growth experiments is plotted against deposition time, showing a positive CLS compared to bulk Pt. For both samples, the Pt 4f $^7/_2$ CLS is observed to be around 1.0 eV at the lowest Pt coverage and decreases most sharply over the first 5 min. At a deposition time of 5 min, corresponding to about 1 ML of Pt deposited, a shift of ~0.45 eV is observed for both samples, consistent with that reported for one pseudomorphic layer of Pt evaporated onto a W(110) substrate.[43]

The origin in CLS in thin metal overlayers has been attributed to a variety of factors, including (i) interatomic charge transfer between the overlayer and the substrate, (ii) intra-atomic charge transfer between orbitals in the overlayer atoms, (iii) charge redistribution, and (iv) differences in final state effects caused by relaxation of electrons around the core-hole.[42] All of these factors result directly or indirectly from bonding between the overlayer atoms and the substrate. Although the presence of the Pt 4f $^7/_2$ CLS in Figure 3c is not direct proof of a Pt ML, it does provide strong evidence that a majority of the deposited Pt atoms are in intimate contact with the WC/W_2C substrates. Supporting this statement is the observation that the notable change in the slope of the CLS curve is located at around 5 min, which corresponds well with the break in the growth curves of Figure 3a,b. This change in slope in Figure 3c can be explained by a decrease in the influence of the factors (i–iv) cited above that can be expected once the first ML is completed.

Because the core level binding energy reflects the electronic and structural states of the Pt overlayer, the Pt 4f $^7/_2$ peak position can serve as an important metric for detecting changes in the Pt overlayer structure resulting from a chemical or electrochemical treatment. For this reason, changes to the Pt 4f $^7/_2$ peak position were closely monitored following extended HER stability tests presented in Section 3.4.

3.3. Comparison of HER Activity of Pt–WC and Pt–W_2C. The HER activity of Pt, WC, W_2C, Pt–WC and Pt–W_2C electrodes was determined by conducting LSV measurements in 0.5 M H_2SO_4 at room temperature. From LSV measure-

dx.doi.org/10.1021/ja208656v | J. Am. Chem.Soc. 2012, 134, 3025–3033

ments, the log of the current density was plotted versus the electrochemical potential to obtain Tafel curves (Figure 4),

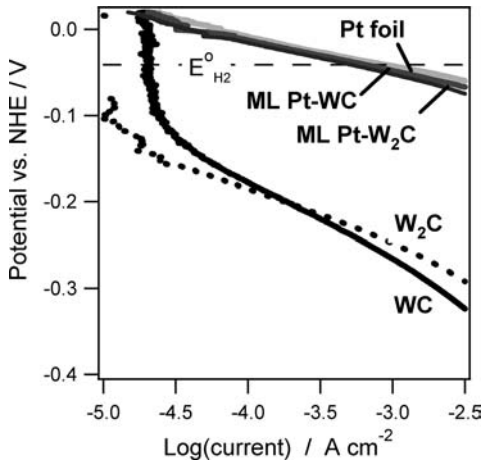

Figure 4. Tafel curves of bare and Pt-modified WC and W_2C thin films in Ar-purged 0.5 M H_2SO_4 at room temperature. For comparison, the Tafel plot for polycrystalline Pt foil is also included.

commonly used for quantitative kinetic analysis of HER catalysts. From the linear region of the Tafel plots, the exchange current densities (i_o) and Tafel slope (β) were determined for each sample and are provided in Table 3.

Table 3. Tafel Parameters Obtained for Different Thin Films from LSV Measurements in Ar-Purged 0.5 M H_2SO_4 Solutions at Room Temperature

sample	$-\log(i_o)$ (A cm^{-2})	$-\beta$ (mV dec^{-1})
Pt foil	−3.1	33
W_2C	−6.7	69
WC	−5.6	91
ML Pt−WC	−3.2	34
ML Pt−W_2C	−3.3	35

Comparison of the Tafel plots in Figure 4 reveals that the carbide surfaces display HER overpotentials that are 200−300 mV greater than the Pt foil. The Tafel parameters obtained for Pt foil are consistent with those reported in literature for polycrystalline Pt in H_2SO_4.[24] For the WC thin film, i_o and β values are slightly lower than those reported for smooth, sintered WC electrodes,[44] likely due to differences in electrode surface areas. No reported Tafel parameters could be found for the W_2C thin film electrode. Despite similarities in the HER overpotentials of the WC and W_2C samples, the Tafel slopes are substantially different (91 mV/dec for WC and 69 mV/dec for W_2C). This deviation in HER behavior may reflect differences in the rate-limiting step on each surface,[45] but more advanced electroanalytical techniques are needed to verify this possibility. Nonetheless, it can be concluded from Figure 4 that single-phase WC and W_2C catalysts having comparable real surface areas display similar HER overpotentials.

As shown in Figure 4, ML Pt−WC and Pt−W_2C surfaces exhibit significant enhancement in HER activity compared to unmodified WC/W_2C, with Tafel curves being nearly identical to bulk Pt. From Table 3, the Tafel parameters for Pt foil are slightly better than ML Pt−WC and Pt−W_2C surfaces, although this minute difference could be caused by differences in crystal orientation, as strong dependence on HER i_o values has been found for the various crystal faces of Pt.[46] Regardless, both ML Pt−WC and Pt−W_2C films show very high HER activity, consistent with predictions based on the DFT-calculated HBE values of these surfaces. The most important observation of Figure 4 is that one ML of Pt on WC/W_2C surfaces can provide HER activity that is comparable to bulk Pt, indicating that Pt loadings in water electrolysis applications may be drastically decreased without compromising efficiency.

3.4. Stability of Pt−WC and Pt−W_2C Surfaces under HER Conditions. For ML electrocatalysts, the most important characteristic is stability of the top monolayer under appropriate operating conditions. Stability is especially critical for subnanometer Pt particles or films, which can be expected to agglomerate into larger, more thermodynamically stable particles in the absence of strong Pt-substrate interactions.[47] Currently, the most common PEM support material is carbon, usually in the form of carbon black.[47] Carbon can be a cheap, high surface area support material, but it is relatively inactive toward the HER, and its slow degradation in acidic environments has been cited as a primary reason for Pt loss in fuel cells.[47,48] In alkaline water electrolysis, it has similarly been found that the low adhesion of Pt to graphite leads to loss of Pt particles during hydrogen evolution.[49] In contrast to carbon, WC/W_2C phases have displayed comparably better stability as support materials in fuel cell applications for Pt nanoparticles[50−52] and Pt ML.[53,54] These findings are consistent with the strong binding energies between Pt and WC/W_2C in Table 2, and lead to the expectation that ML Pt display good stability on the carbide substrates.

For bulk WC/W_2C and Pt electrocatalysts, a primary concern in electrochemical applications is their oxidation to oxides or dissolution into the electrolyte. Fortunately, the negative potentials of a HER cathode are generally not conducive to electro-oxidation of these materials. Pt is one of the more stable electrocatalyst materials, with Pt oxidation/dissolution typically not observed for potentials <0.85 V RHE in acidic conditions.[55] Although carbide phases do not possess the same superb corrosion resistance as Pt, both W_2C and WC display oxidation onset potentials that are significantly more positive than RHE,[56] meaning neither carbide should be susceptible to sustained corrosion under HER operating potentials. As expected, XPS scans of the W 4f region for both unmodified WC/W_2C surfaces following chronopotentiometry (CP) measurements under HER conditions reveal negligible W 4f oxide features (see Supporting Information). The stable nature of the tungsten carbide films under HER conditions is consistent with recent stability studies of WC and W_2C surfaces over wide pH and potential ranges.[57,58]

Although the very positive standard reduction potential for Pt ensures that ML Pt is not vulnerable to anodic dissolution under HER conditions, there is concern that poor adhesion of the Pt ML to a given substrate will lead to detachment and/or agglomeration of Pt. Because all Pt atoms in a ML structure are exposed to the electrolyte, minor detachment or agglomeration of small portions of the Pt ML would result in significant loss of active surface area and a corresponding decrease in HER activity. Results in DFT calculations presented in Table 2 indicated strong adhesion of ML Pt to the WC/W_2C surfaces, but these calculations do not take into account the possible influences of the interaction with the aqueous electrolyte and H_2 bubble formation/cavitation.

To test the stability of ML Pt on WC/W_2C surfaces in this work, LSV measurements were recorded before and after a

dx.doi.org/10.1021/ja208656v | J. Am. Chem.Soc. 2012, 134, 3025−3033

series of chronopotentiometry (CP) measurements to simulate on/off operation in an electrolysis device. CP measurements consisted of alternating induced current densities of 0.0 mA cm^{-2} (5 min) and −10.0 mA cm^{-2} (25 min) over 2 h. During CP measurements, the overpotential of the working electrode was monitored as a function of time, as shown for ML Pt−WC and Pt−W_2C surfaces in Figure 5, panels a and b, respectively.

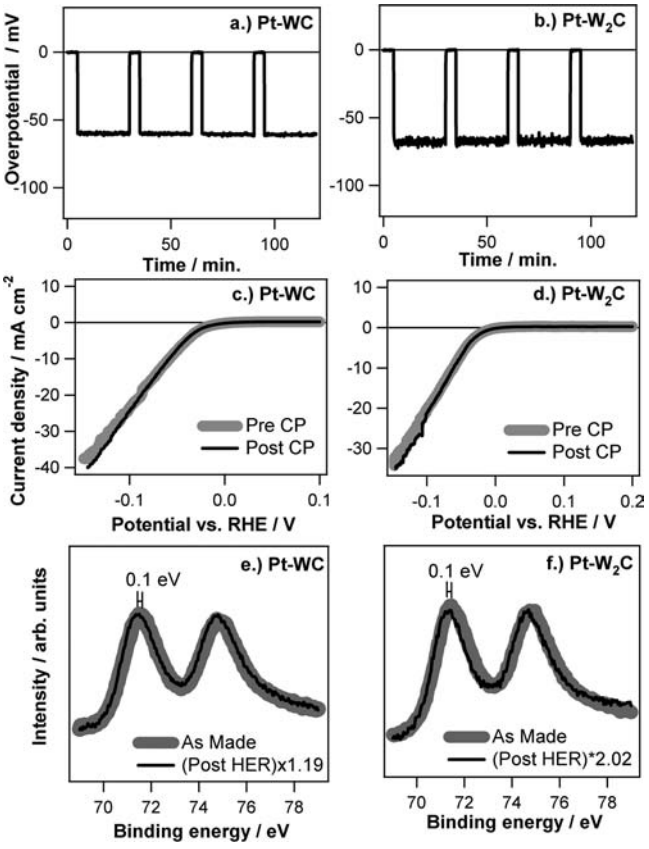

Figure 5. Results of stability tests for ML Pt−WC and ML Pt−W_2C thin films. (a and b) CP stability tests performed in H_2-purged 0.5 M H_2SO_4 at room temperature over 2 h. The current was alternated between 0.0 and 10 mA cm^{-2} to simulate electrolyzer operation. (c and d) LSV measurements taken before and after the CP measurement. (e and f) Pt 4f region following extended stability tests conducted in H_2-purged 0.5 M H_2SO_4 at room temperature.

For both electrodes, constant HER overpotentials of ∼60 mV were recorded during the current withdrawing steps and the potential assumed the value of the reversible hydrogen electrode (RHE) during the open circuit steps. The constant overpotential in this CP measurement is characteristic of stable cathodic operation,[49] which suggests that the structure of the Pt ML has not changed. In Figure 5c,d, stable HER activity is verified by the observation that LSV measurements recorded before and after CP measurements are essentially identical.

XPS and SEM measurements of the ML Pt−WC and Pt−W_2C surfaces were conducted before and after the CP measurements to further verify the stability of the Pt overlayer. XPS scans following HER measurements confirmed the absence of any contaminants on the surfaces, which can have a strong influence on HER behavior. In Figure 5e,f the Pt 4f spectra of surfaces taken following CP/LSV measurements are superimposed to those of the as-synthesized samples. For both Pt−WC and Pt−W_2C, the normalized Pt 4f spectra are nearly identical in shape and position, indicating no change in the electronic properties of the Pt overlayer as discussed in Section 3.2. This in turn infers no change in the structure of the Pt overlayer. Equally important is the finding that the Pt 4f/W 4f peak ratios taken before and after extended stability tests do not change for either catalyst (Supporting Information). If there were a loss of Pt from the surface or agglomeration of Pt to form particles, the Pt/W ratio would be expected to decrease. Further evidence of the stability of the Pt−WC/W_2C surfaces is provided by high-resolution SEM images taken following CP measurements (Supporting Information). The absence of discernible Pt particles in the SEM images is consistent with conclusion of the Pt ML stability from the electrochemical and XPS measurements.

3.5. Investigation of Other ML Metal−TMC Electrocatalysts. In addition to the ML Pt−(WC/W_2C) surfaces, the HER activity was also investigated for the following metal−TMC surfaces whose HBE values span a wide range of the HER volcano curve: Mo_2C, ML Pd−Mo_2C, ML Pd−WC, ML Au−Mo_2C, and ML Au−WC. The DFT-calculated HBE values for these surfaces were listed in Table 1. Among these additional surfaces, Mo_2C is one of the most commonly studied TMCs and has shown promising catalytic activity in both gas-phase reaction systems and electrocatalytic applications.[5] Furthermore, the onset for oxidation of single-phase Mo_2C thin films in an acidic environment is not observed until +0.4 V RHE,[11] a potential that is well positive of HER operating potentials. For overlayer metals, Au was selected for the purpose of investigating catalysts located on the low HBE side of the volcano curve (Au−WC and Au), while Pd was chosen due to reported high HER activity of previously studied ML Pd bimetallic surfaces.[22,59] Furthermore, the price of Pd is currently less than 50% that of Pt,[8] making ML Pd−TMC HER catalysts especially attractive from a cost standpoint.

The HER activity of each of the surfaces was measured as already described for the ML Pt−WC and Pt−W_2C surfaces. In Figure 6, the i_o values determined from the Tafel plots for these surfaces are plotted versus the corresponding DFT-calculated HBE. Also included are the data points for WC/W_2C, Pt, Pt−WC, and Pt−W_2C surfaces. It is apparent that a volcano relationship is observed for the surfaces studied in this work, reflecting Sabatier's principle as discussed earlier. Previous DFT studies have shown that both pure metals[24] and ML bimetallic surfaces[22] display a volcano relationship between HER activity and HBE. Figure 6 provides evidence that TMC and metal-modified TMC surfaces also obey a similar volcano relationship. The importance of this finding is that other ML−TMC surfaces may be effectively screened for HER activity based on their DFT-calculated HBE values.

Of the additional surfaces studied, the ML Pd−WC and ML Pd−Mo_2C thin films showed the most promise as HER electrocatalysts. Although their measured HER activity was not as high as bulk Pt or Pd films, their relatively high activity, potential for synthesis of high surface area structures (for Mo_2C), and the lower cost of Pd compared to Pt warrant further development of these catalysts. Slightly lower HER activity may be tolerated for low-current density electrolysis applications such as photoelectrochemical cells or photovoltaic electrolysis, especially if a low-cost, high surface area substrate material such as Mo_2C can be used.

3.6. Opportunities and Challenges for Commercial Application. This study has focused on well-controlled ML metal−TMC thin film surfaces, but the thin film electrode

dx.doi.org/10.1021/ja208656v | J. Am. Chem.Soc. 2012, 134, 3025−3033

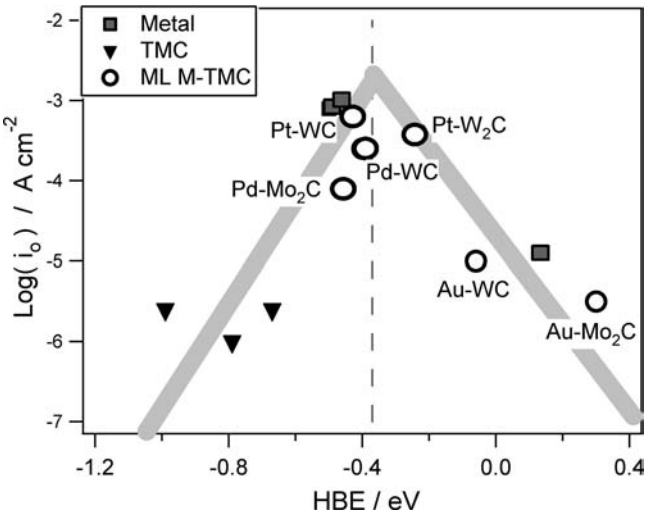

Figure 6. Volcano relationship between HER activity (i_o) and hydrogen binding energy (HBE) for all metal, TMC, and ML-metal–TMC thin films studied in this work. The i_o values were obtained from Tafel analysis of linear sweep voltammograms performed in H_2-purged 0.5 M H_2SO_4 at room temperature, while HBE values are taken from Table 1. Thick gray lines are included to guide the eye while the dashed gray line marks the center of the volcano curve, located 0.09 eV more positive than the HBE of Pt(111) according to Noskov et al.[24]

geometry is not suitable for electrolysis applications beyond low-current density photoelectrochemical and PV electrolysis cells. For high rates of water electrolysis in a PEM electrolyzer, high surface area particulate or mesoporous materials with a ML metal/TMC core/shell structure are needed. Synthesis of such core–shell structures presents several challenges, including deposition/synthesis of uniform metal shells, achieving good control of the metal–TMC interface, and synthesizing TMC structures with high surface areas. Thermal evaporation on TMC thin films was suitable in this work, but vacuum processing steps are generally not conducive to scaled-up production processes and line-of-site deposition techniques are not capable of uniformly coating 3-dimensional materials. For these reasons, alternative synthesis methods, including but not limited to atomic layer deposition, reverse micelle synthesis, and chemical vapor deposition, must be explored. Through careful design of processing steps and knowledge gained from thin film studies, it should be possible to produce low-cost ML metal–TMC core–shell catalysts that are suitable for high current density electrolysis applications.

4. CONCLUSIONS

Well-characterized, single-phase WC, W_2C, and Mo_2C thin film electrodes have been studied as a platform for comparing the utility of these materials as supports for ML-thick precious metal HER catalysts. In electrochemical measurements, both WC and W_2C surfaces were shown to be excellent supports for ML amounts of Pt, with demonstrated HER activities that are comparable to bulk Pt, consistent with predictions based on DFT-calculated hydrogen binding energies for ML Pt–WC and Pt–W_2C. More importantly, a combination of electroanalytical, XPS, and SEM measurements were used to show that these catalysts are stable over 2 h of HER operation at an HER current density of 10 mA cm^{-2}. This study has also shown that multiple combinations of ML metals supported on TMC substrates obey the commonly observed volcano relationship between HER activity and HBE. In future research efforts, the single-phase TMC thin films studied here can serve as a useful experimental platform for elucidating the roles of defects, surface carbon, and oxide species on the metal ML–TMC interface. Such investigations will lead to a better understanding of the interactions of metal overlayers with TMC surfaces, allowing for the optimization of catalyst activity/stability while enabling translation of that knowledge to high surface area mesoporous and particulate catalysts for high current density electrolysis applications. Results from the current study demonstrate the proof-of-principle of using monolayer Pt–WC and Pt–W_2C thin films as active and stable electrolysis catalysts. Additional studies with much longer duration and on Pt–WC and Pt–W_2C powder catalysts would be needed to verify the commercial feasibility of this class of promising HER electrocatalysts.

■ ASSOCIATED CONTENT

Supporting Information

Sample synthesis, detailed characterization results, and description of testing procedures. This material is available free of charge via the Internet at http://pubs.acs.org.

■ AUTHOR INFORMATION

Corresponding Author

jgchen@udel.edu

■ ACKNOWLEDGMENTS

We acknowledge financial support from the Department of Energy (DE-FG02-00ER15104). We acknowledge Brian McCandless for assistance with XRD and GIXRD, Irene Hsu for assistance with thin film synthesis, and Kevin Dobson for discussion.

■ REFERENCES

(1) Rajeshwar, K.; McConnell, R.; Harrison, K.; Licht, S. In *Solar Hydrogen Generation*; Rajeshwar, K., McConnell, R., Licht, S., Eds.; Springer Science & Business Media: New York, 2008; p 11.
(2) Harrison, K.; Levene, J. I. In *Solar Hydrogen Generation: Toward a Renewable Energy Future*; Rajeshwar, K., McConnell, R., Licht, S., Eds.; Springer Science & Business Media: New York, 2008; pp 41–63.
(3) Grigoriev, S. A.; Millet, P.; Fateev, V. N. *J. Power Sources* **2008**, *177*, 281–285.
(4) Yang, C. J. *Energy Policy* **2009**, *37*, 1805–1808.
(5) Hwu, H. H.; Chen, J. G. *Chem. Rev.* **2005**, *105*, 185–212.
(6) WebElements Home Page. www.webelements.com (accessed June 2011).
(7) Metal-Pages Home Page. www.metal-pages.com (accessed June 2011).
(8) Platinum Today Home Page. http://www.platinum.matthey.com/pgm-prices/price-charts/ (accessed June 2011).
(9) Bozzini, B.; De Gaudenzi, G. P.; Fanigliulo, A.; Mele, C. *Corros. Sci.* **2004**, *46*, 453–469.
(10) Zellner, M. B.; Chen, J. G. *Surf. Sci.* **2004**, *569*, 89–98.
(11) Weigert, E. C.; Esposito, D. V.; Chen, J. G. *J. Power Sources* **2009**, *193*, 501–506.
(12) Nikolov, I.; Petrov, K.; Vitanov, T.; Guschev, A. *Int. J. Hydrogen Energy* **1983**, *8*, 437–440.
(13) Sokolsky, D. V.; Palanker, V. S.; Baybatyrov, E. N. *Electrochim. Acta* **1975**, *20*, 71–77.
(14) Bohm, H. *Electrochim. Acta* **1970**, *15*, 1273-&.
(15) Harnisch, F.; Sievers, G.; Schroder, U. *Appl. Catal., B* **2009**, *89*, 455–458.

(16) Ma, C.; Sheng, J.; Brandon, N.; Zhang, C.; Li, G. *Int. J. Hydrogen Energy* **2007**, *32*, 2824−2829.
(17) Wu, M.; Shen, P. K.; Wei, Z. D.; Song, S. Q.; Nie, M. *J. Power Sources* **2007**, *166*, 310−316.
(18) Ham, D. J.; Ganesan, R.; Lee, J. S. *Int. J. Hydrogen Energy* **2008**, *33*, 6865−6872.
(19) Chen, J. G.; Menning, C. A.; Zellner, M. B. *Surf. Sci. Rep.* **2008**, *63*, 201−254.
(20) Esposito, D. V.; Hunt, S. T.; Stottlemyer, A. L.; Dobson, K. D.; McCandless, B. E.; Birkmire, R. W.; Chen, J. G. *Angew. Chem., Int. Ed.* **2010**, *49*, 9859−9862.
(21) Greeley, J.; Jaramillo, T. F.; Bonde, J.; Chorkendorff, I. B.; Norskov, J. K. *Nat. Mater.* **2006**, *5*, 909−913.
(22) Greeley, J.; Norskov, J. K.; Kibler, L. A.; El-Aziz, A. M.; Kolb, D. M. *ChemPhysChem* **2006**, *7*, 1032−1035.
(23) Greeley, J.; Stephens, I. E. L.; Bondarenko, A. S.; Johansson, T. P.; Hansen, H. A.; Jaramillo, T. F.; Rossmeisl, J.; Chorkendorff, I.; Norskov, J. K. *Nat. Chem.* **2009**, *1*, 552−556.
(24) Norskov, J. K.; Bligaard, T.; Logadottir, A.; Kitchin, J. R.; Chen, J. G.; Pandelov, S.; Norskov, J. K. *J. Electrochem. Soc.* **2005**, *152*, J23−J26.
(25) Moulder, J. F.; Stickle, W. F.; Sobol, P. E.; Bomben, K. D. *Handbook of X-ray Photoelectron Spectroscopy*; Physical Electronics, Inc.: Eden Prairie, MN, 1995.
(26) Sabatier, P. *Catalysis in Organic Chemistry*; D. Van Nostrand Company: New York, 1922.
(27) Kita, H. *J. Electrochem. Soc.* **1966**, *113*, 1095−1111.
(28) Trasatti, S. *J. Electroanal. Chem.* **1972**, *39*, 163−184.
(29) Menning, C. A.; Chen, J. G. *J. Chem. Phys.* **2009**, *130*, 1−7.
(30) Wang, L. L.; Johnson, D. D. *J. Am. Chem. Soc.* **2009**, *131*, 14023−14029.
(31) Campbell, C. T. *Annu. Rev. Phys. Chem.* **1990**, *41*, 775−837.
(32) Zhou, Z. H.; Gao, F.; Goodman, D. W. *Surf. Sci.* **2010**, *604*, 1071−L38.
(33) Kittel, C.; McEuen, P. *Introduction to Solid State Physics*, 8th ed.; J. Wiley: Hoboken, NJ, 2005.
(34) Cullity, B. D. In *Elements of X-ray Diffraction*; Cohen, M., Ed.; Addison-Wesley: Reading, MA, 1956; pp 272−275.
(35) Esposito, D. V.; Dobson, K. D.; McCandless, B. E.; Birkmire, R. W.; Chen, J. G. *J. Electrochem. Soc.* **2009**, *156*, B962−B969.
(36) Ross, P. N.; Stonehart, P. *J. Catal.* **1977**, *48*, 42−59.
(37) Johansson, L. I. *Surf. Sci. Rep.* **1995**, *21*, 179−250.
(38) Leclercq, L.; Almazouari, A.; Dufour, M.; Leclercq, G. In *The Chemistry of Transition Metal Carbides and Nitrides*; Oyama, S. T., Ed.; Blackie: Glasgow, 1996; pp 345−361.
(39) Leclercq, G.; Kamal, M.; Giraudon, J. M.; Devassine, P.; Feigenbaum, L.; Leclercq, L.; Frennet, A.; Bastin, J. M.; Lofberg, A.; Decker, S.; Dufour, M. *J. Catal.* **1996**, *158*, 142−169.
(40) Rhead, G. E.; Barthes, M. G.; Argile, C. *Thin Solid Films* **1981**, *82*, 201−211.
(41) Humbert, M. P.; Menning, C. A.; Chen, J. G. *J. Catal.* **2010**, *271*, 132−139.
(42) Weinert, M.; Watson, R. E. *Phys. Rev. B* **1995**, *51*, 17168−17180.
(43) Riffe, D. M.; Shinn, N. D.; Kim, B.; Kim, K. J.; Kang, T. H. *Surf. Sci.* **2009**, *603*, 3431−3438.
(44) Tsirlina, G. A.; Petrii, O. A. *Soviet Electrochem.* **1985**, *21*, 653−660.
(45) Bockris, J. O. M.; Reddy, A. K. N.; Gamboa-Aldeco, M. In *Modern Electrochemistry*; 2nd ed.; Plenum Press: New York, 1998; pp 211−405.
(46) Barber, J.; Morin, S.; Conway, B. E. *J. Electroanal. Chem.* **1998**, *446*, 125−138.
(47) Shao-Horn, Y.; Sheng, W. C.; Chen, S.; Ferreira, P. J.; Holby, E. F.; Morgan, D. *Top. Catal.* **2007**, *46*, 285−305.
(48) Shao, Y. Y.; Wang, J.; Kou, R.; Engelhard, M.; Liu, J.; Wang, Y.; Lin, Y. H. *Electrochim. Acta* **2009**, *54*, 3109−3114.
(49) Dabo, P.; Fournier, J.; Brossard, L.; Menard, H.; Magny, P.; Mahdavi, B. *Int. J. Hydrogen Energy* **1998**, *23*, 167−175.
(50) Shao, Y. Y.; Liu, J.; Wang, Y.; Lin, Y. H. *J. Mater. Chem.* **2009**, *19*, 46−59.
(51) Chhina, H.; Campbell, S.; Kesler, O. *J. Power Sources* **2007**, *164*, 431−440.
(52) Bosco, J. P.; Sasaki, K.; Sadakane, M.; Ueda, W.; Chen, J. G. *Chem. Mater.* **2010**, *22*, 966−973.
(53) Weigert, E. C.; Stottlemyer, A. L.; Zellner, M. B.; Chen, J. G. *J. Phys. Chem. C* **2007**, *111*, 14617−14620.
(54) Weigert, E. C.; Zellner, M. B.; Stottlemyer, A. L.; Chen, J. G. *Top. Catal.* **2007**, *46*, 349−357.
(55) Ferreira, P. J.; la, O', G. J.; Shao-Horn, Y.; Morgan, D.; Makharia, R.; Kocha, S.; Gasteiger, H. A. *J. Electrochem. Soc.* **2005**, *152*, A2256−A2271.
(56) Zellner, M. B.; Chen, J. G. *Catal. Today* **2005**, *99*, 299−307.
(57) Weidman, M. C.; Esposito, D. V.; Hsu, I. J.; Chen, J. G. *J. Electrochem. Soc.* **2010**, *157*, F179−F188.
(58) Weidman, M. C.; Esposito, D. V.; Hsu, Y.-C.; Chen, J. G. *J. Power Sources* **2012**, *202*, 11−17.
(59) Wolfschmidt, H.; Weingarth, D.; Stimming, U. *ChemPhysChem* **2010**, *11*, 1533−1541.